Structural studies of amorphous titanium diboride thin films by extended x-ray-absorption fine-structure and extended electron-energy-loss fine-structure techniques

Alain E. Kaloyeros
Physics Department, State University of New York at Albany, Albany, New York 12222

Mark P. Hoffman, Wendell S. Williams,* Alex E. Greene, and Joyce A. McMillan
Department of Physics and Materials Research Laboratory, University of Illinois at Urbana-Champaign, 1110 West Green Street, Urbana, Illinois 61801

(Received 24 March 1988)

The local atomic structure of amorphous titanium diboride thin films, prepared by electron-beam vaporization (EBV) of the crystalline compound onto liquid-nitrogen-cooled substrates, was studied using extended x-ray-absorption fine-structure (EXAFS) and extended energy-loss fine-structure (EXELFS) techniques. From a comparison of the extended fine-structure spectra of the amorphous films with corresponding spectra of crystalline titanium diboride, accurate information was derived on the nature of the local structure, or short-range order, and on the coordination numbers, interatomic distances, and nanostructural atomic disorder in amorphous TiB_2. A relaxation of the interatomic spacing and a reduction of coordination number for the nearest-neighbor atoms was inferred for the amorphous state. Local prismatic coordination with random 90° rotations about prismatic planes is proposed as a likely atomic structure consistent with the data for the amorphous form. Finally, EXAFS and EXELFS were employed to examine in detail the structural changes induced in amorphous TiB_2 by variations in the EBV deposition parameters, and to determine a set of optimized parameters for the EBV deposition of a TiB_2 stable amorphous phase.

I. INTRODUCTION

Amorphous alloys and compounds of the transition metals and the metalloid elements (boron and carbon) constitute an interesting and rapidly developing branch of the family of disordered solids.[1,2] These materials can be prepared by a variety of techniques, and their properties are sufficiently remarkable to warrant technological applications and industrial utilization.[3] Because they combine availability, interesting properties, and usefulness, their structure and properties have become an important area of theoretical and experimental physics research.[4]

Although crystallization at modest temperatures limits the practical usefulness of most glassy metals,[5] stability to much higher temperatures has been achieved by the authors for amorphous films of titanium carbide, TiC.[6–11] In the present study we examine amorphous films of titanium diboride, TiB_2.

In its crystalline form, titanium diboride is a refactory, metallic, essentially stoichiometric compound with a high melting point (~2980 °C) and good electrical conductivity.[12] It exhibits extreme chemical stability and excellent resistance to corrosion.[13] Such properties have made TiB_2 an interesting compound from the scientific standpoint and a promising candidate for many engineering applications under aggressive environmental conditions. Present industrial interest in TiB_2 recognizes its potential for use as an abrasive, as a protective coating, as a possible high-temperature electrode in the refining of aluminum, as a component in composites, and, like all boron-containing substances, as a potential material for use as a neutron absorber.[14–16] One reason for undertaking this investigation was our expectation that these advantageous properties of TiB_2 could be enhanced or extended by preparing it in an amorphous form, leading to an even broader range of technological applications.[17]

For example, TiB_2 appears attractive for use in the microelectronics industry as a diffusion barrier for integrated-circuit metallization. Although this possibility was suggested as far back as 1969, little work has been reported since then on using it for this application.[18,19] This neglect may, in part, result from the complex requirements for integrated-circuit development, in particular, the need to minimize high-temperature processing and to maximize step-coverage quality. These conditions impose very stringent limitations on the standard technique for producing TiB_2 films, chemical-vapor deposition (CVD), which uses hydrogen reduction of the chlorides: the chemical reaction becomes thermodynamically favorable only at high temperatures (above 900 °C), and a large amount of hydrochloric acid is produced.[20] Both conditions are extremely detrimental to integrated circuit components as well as to many substrates. Preparation of TiB_2 films by methods which deposit amorphous material seems to be a very promising approach to circumventing these problems since the experimental technique involved requires cooling the substrate to low temperatures where the thermal energy for the differential steps required in crystallization is not available.[10] Furthermore, this technique does not produce any hydrochloric acid by-products. This potential application of amorphous titanium diboride films to the fabrication of electronic devices could lead to substantial economies.

This paper is one in a series of reports by the present authors on the successful preparation, characterization, and study of the structure and properties of amorphous

TiB_2 thin films. We focus here on the identification of structural arrangements of atoms in the amorphous phase, since knowledge of the local atomic environment, and of any nanostructural static disorder is of great value in interpreting the electrical, optical, and mechanical properties.[21,22]

Results of structural investigations by extended x-ray-absorption fine-structure (EXAFS) and extended electron-energy-loss fine-structure (EXELFS) techniques are presented for amorphous TiB_2 thin films produced, at this preliminary stage of our work, by electron-beam vaporization (EBV), since TiB_2 vaporizes congurently.[23] Information generated on the static atomic displacement and the local atomic environment of both the metalloid (from the B K-edge EXELFS), and metal (from the Ti K-edge EXAFS), and on the nature and degree of short-range order (SRO) in the amorphous TiB_2 phase, is presented and discussed in relation to the basic structural units of its crystalline form. In particular, we show that short-range order does indeed exist in the amorphous phase at the level of the first and second boron and titanium coordination shells, a result to be contrasted with amorphous titanium carbide films, where no chemical ordering was detected beyond the first carbon and titanium coordination shells.[24] The degree of this local (chemical) ordering in the TiB_2 amorphous phase depends strongly on the deposition parameters used during EBV. We also demonstrate that the EXAFS-EXELFS combination is a powerful tool for probing the local atom environment in amorphous solids and in compounds composed of both light and heavy constituents.

II. EXPERIMENT

The initial method chosen for preparing amorphous TiB_2 was vaporization of a crystalline specimen onto a cooled substrate using electron-beam vaporization (EBV). The source material for the EBV process consisted of high-purity (99.999%) chips of TiB_2 single crystals, placed in the water-cooled hearth of the EBV evaporator. Compound TiB_2 targets, rather than separate elemental targets, were used as titanium diboride vaporizes congruently,[23] whereas born does not vaporize exclusively as a monatomic species from elemental boron.[25] The pressure in the vaporization chamber was kept below $\sim 10^{-7}$ torr at all times, and the electron-beam voltage was varied, for different deposition runs, from 6 to 9 kV with a power rating of 20–40 kW. Although the temperature of the target during vaporization is not known precisely, it was in the range 2000–25000 °C. The TiB_2 coatings were deposited onto Pyrex and quartz glass substrates and cooled to liquid-nitrogen temperature. The films produced were of uniform thickness, silver-colored, mirror-bright, and adherent. The film thickness, determined by profiling with an α-step analyzer (2×10^{-3}-μm resolution), was 0.5–1 μm.

The EXAFS and EXELFS studies were carried out at the Center for the Microanalysis of Materials, Materials Research Laboratory, University of Illinois at Urbana-Champaign.

The transmission EXAFS studies were carried out using x rays produced by a Rigaku RU-200 laboratory rotating-anode x-ray generator, equipped with a molybdenum target and operated at 12–13 kV with a beam intensity ~ 70 mA. This high intensity allows EXAFS spectra to be collected on a time scale of a few hours, thus reducing the effects of source instability to a minimum.[26] Extreme care was taken to eliminate impurity wavelengths from the source, i.e., higher-order x-ray excitations, by combining the choice of an x-ray excitation voltage below the threshold for emission of such wavelengths with the use of a focusing Johansson curved-crystal monochromator. The detection system consists of a beam monitor placed in front of the sample, to measure the incident-beam intensity, $\mathcal{I}_0$, and of a beam detector positioned behind the sample to collect the transmitted signal, $\mathcal{I}$. This configuration permits simultaneous detection of $\mathcal{I}$ and $\mathcal{I}_0$, subsequently, the compilation of difference spectra from the normalized ratio $\mathcal{I}_0/\mathcal{I}$, thus eliminating any errors induced by time-dependent fluctuations in the source or mechanical wobble in the spectrometer.[27] Finally, a GSK Scientific model 100 EXAFS cold stage was employed to collect spectra from samples cooled by liquid nitrogen to reduce thermal vibration effects.[28,29]

Considerable attention was also devoted to eliminating other experimental sources of error in EXAFS measurements, which include cracks or holes in the sample, where a fraction of the incident beam can pass unaffected by a jump in the absorption edge, and particle-size and thickness effects in powdered samples and thin films.[30] An optimum thickness was determined experimentally by collecting EXAFS data for crystalline TiB_2 films and powdered samples of various thicknesses and particle sizes, then performing the entire data analysis and comparing the experimentally determined structural parameters with the standard crystalline values.[31] We found that a film thickness—or particle size—of 5–7.5 μm was needed to achieve best results. Special precaution was also taken to prepare amorphous TiB_2 powedered standard samples. The amorphous films were removed from the substrates by etching with hydrofluoric acid, and 10–15 layers were collected on cellophane tape to make samples of optimum thickness. The crystalline TiB_2 samples, in the form of powders, were ground and sieved to 400 mesh to assure small grain texture. These powders were also mounted on transparent cellophane tape.

The EXELFS measurements employing a high-energy electron beam (300 keV) were performed on a Philips EM430 transmission electron microscopic (TEM) combined with a Gatan model 607 single-magnetic-sector, double-focusing electron-energy-loss spectrometer. The electron microscope was used in the bright-field imaging mode to form a 1-μm-diam probe of 300-keV electrons on the speciment with a beam current of ~ 1 μA. An entrance slit to the spectrometer selects according to their scattering angle and the spectrometer disperses them in a direction perpendicular to the slit. Spectra are recorded by scanning the energy-loss intensity across an apertured scintillator (model NE100) and by counting the single pulses derived from the photomultiplier (RCA 8575).[32]

In the case of EXELFS measurements using an electron-beam source, we optimized instrumentation fac-

tors such as the electron probe current I, its diameter on the sample, the energy resolution and acceptance angle of the spectrometer, and the total dwell time needed per eV channel. Following the procedure of Leapman, Grunes, Fejes, and Silcox,[33] we performed a check of the reliability of the counting rates achievable with our system and of ways for optimizing them for different sets of typical experimental parameters. We made use of standard expressions for count rates of scattered electrons which have been analyzed by a spectrometer and have lost an energy E through core-level excitations, and of calculated oscillator-strength data given by Leapman, Rez, and Mayers[32] for the excitations just above the B and Ti K-shell ionization edges. We found that for a typical 10-nm-thick sample analyzed with an electron beam of 300 keV, which forms a probe on the sample with a diameter of 1 μm, and a total probe current of 1 μA, and using an electron-energy-loss spectrometer designed to accept electrons scattered inside a semiangle of 10 mrad with an energy resolution of 3 eV, counting rates as high as 10^5-10^6 counts per eV channel are achievable. However, the exponential nature of the EXELFS spectrum decay above threshold makes it necessary to collect data for a longer time. For this reason, sweeps of individual spectra were compiled to give a total counting time of 3–4 s per eV channel. Digital scans of 0–50 eV were thus controlled by an EDAX 9100/60 minicomputer, which was also used to store the spectra and perform the initial data processing and background subtraction. Since the spectrometer is capable of $\sim$1-eV resolution, the energy resolution of the measured spectra ($\sim$3 eV) was determined mainly by the thermal spread of the incident beam. Thermal vibrations were reduced by mounting the TEM samples in a Philips-mode PWG591/01 side-entry cold stage and collecting spectra at liquid-nitrogen temperature. Multiple-scattering effects, such as collective plasmons, were also minimized by limiting the sample thickness to $\sim 1.5\lambda$ (where λ is the inelastic mean free path), leading to typical thicknesses of 1000–2000 Å).

III. EXAFS-EXELFS FORMALISM AND DATA ANALYSIS

Extended x-ray-absorption fine structure (EXAFS) is the oscillatory modulation of the absorption coefficient on the high-energy side of an x-ray-absorption edge of a constituent atom in a material.[34] The EXAFS oscillations are a final-state photoelectron effect arising from the interference between the outgoing photoejected electron wave and the backscattered waves from neighboring atomic sites.[35] The equation for the EXAFS modulation $\chi(k)$, assuming no multiple scattering, and using the formalism of Stern, Sayers, and Lytle,[36] is given by

$$\chi(k)=\frac{\mu(k)-\mu_0(k)}{\mu_0(k)}$$

$$=\sum_j \frac{N_j A_j}{kR_j^2} e^{-2k^2\sigma_j^2} e^{-2R_j/\lambda} \sin(2kR_j+\delta_j) , \quad (1)$$

where $\mu(k)$ is the total absorption coefficient measured above the edge and $\mu_0(k)$ is the smoothly varying atomic contribution. The summation is over coordination shells of atoms surrounding the excited atom, with N_j (the coordination number) atoms in shell j located at an average distance R_j from the central atom. The first exponential term containing σ_j^2 is a Debye-Waller–type term, where σ_j^2 is the mean-square relative positional displacement of the central and backscattering atoms from both thermal disorder and structural disorder. The quantity λ is the phenomenological mean free path that corresponds to a finite lifetime of the excited state, $A_j(2k)$ is the backscattering amplitude of the atoms in the jth shell, and $\delta_j(k)$ is the phase shift experienced by the photoelectron as it traverses the potential of the central and backscattering atoms. The variable k is the ejected photoelectron wave vector.

Since EXAFS is sensitive mainly to short-range order, there is no fundamental distinction between crystals with long-range order and disordered systems, such as aperiodic solids, liquids, and solutions.[37] This feature makes EXAFS an extremely suitable spectroscopy for gaining a fundamental understanding of the structure of amorphous materials, such as amorphous TiB_2.[38]

However, whereas the 4960-eV K edge of titanium is readily detectable with our laboratory rotating-anode x-ray source, the lack of monochromatic radiation of sufficient resolution and intensity from such a source for the 188-eV B K edge made it necessary to search for an alternative measurement method. Although this limitation can be overcome by utilizing a synchrotron-radiation source with its appreciably higher beam intensity, the need to use both grating and crystal monochromators to detect signals from low-atomic-number-Z elements, and the inconvenience of traveling to a synchrotron facility, made it more advantageous to exploit the features of extended electron-energy-loss fine-structure (EXELFS) spectroscopy using an available analytical electron microscope.[39]

EXELFS is the modulation in the differential inelastic-electron-scattering cross section past an ionization edge of a constituent element in a compound.[40] EXELFS, in the case of forward scattering ($k\sim 0$, where k is the electron wave vector), has the same physical origins,[41] contains the same kind of information, is described by the same equation [see Eq. (1)], and can be analyzed in the same way as EXAFS, using the formulation of Stern, Sayers, and Lytle.[36]

The general method of EXELFS involves a monoenergetic beam of electrons which passes through a thin specimen. Electrons interact with atoms in the specimen and are transmitted with a certain loss of energy indicative of the interaction. With the aid of an electron spectrometer, one can study the energy-loss distribution of the transmitted electrons.[42] Since it is a direct measurement of electron scattering, and because it exhibits a one-to-one correspondence between atoms excited by incident electrons and electrons having a characteristic energy loss (under the assumption of single scattering), EXELFS is particularly appropriate for the study of light elements,[43] such as the 188-eV B K edge. In this respect, EXELFS spectroscopy complements and expands the features displayed by its EXAFS counterpart, especially

in compounds composed of both light and heavy constituents, such as titanium diboride.

To extract information from the EXAFS and EXELFS fine-structure spectra, the parameters from Eq. (1) are used. For any given coordination shell j, the corresponding expression,

$$\chi_j(k)=\frac{N_j A_j(k)}{kR_j^2}e^{-2k^2\sigma_j^2}e^{-2R_j/\lambda}\sin(2kR_j+\delta_j)\ , \qquad (2)$$

can be extracted from the data following standard procedures.[36,37] Some of the parameters can be calculated from theory—for instance, we can use theoretical values for the atomic phase shifts given by Teo and Lee[44]— or determined by experimental fitting procedures, but the results are not always satisfactory. Fortunately, when dealing with amorphous materials, we can use the crystalline compound as a standard.[45] The chemical transferability of the phase shifts and backscattering amplitudes is well established, since the local environment and chemical state (local bonding) should not differ much between crystalline and amorphous states.[46] We would expect however, some relaxation in the nearest-neighbor distances and a reduction in the coordination number.

Once we have obtained the $\chi(k)$ functions for the standard, $\chi_s(k)$, and the unknown, $\chi_\mu(k)$, we can separate numerically the phase factor for a particular shell, $\Phi_j=2kR_j+\delta_j(k)$, and take the difference, giving[47]

$$\Phi_u(k)-\Phi_s(k)=2k(R_u-R_s)+[\delta_u(k)-\delta_s(k)]\ , \qquad (3)$$

but because phase shift due to atomic potentials, $\delta_j(k)$, results from comparable chemical environments in the amorphous and the crystalline state, the difference $\delta_u(k)-\delta_s(k)$ is negligible. A plot of $\Phi_u-\Phi_s$ versus $2k$ should therefore produce a straight line with a slope of R_u-R_s and a zero intercept.

Similarly, isolating the amplitudes for the standard and unknown, computing the ratio, and taking the logarithm gives[48]

$$\ln\left[\frac{H_u}{H_s}\right]=-2k^2(\sigma_u^2-\sigma_s^2)-\frac{2}{\lambda}(R_u-R_s)+\ln\left[\frac{N_uR_s}{N_sR_u}\right]\ , \qquad (4)$$

where $H_j=(N_jA_j/R_j^2)\exp(-2k^2\sigma_j^2-2R_j/\lambda)$. The difference R_s-R_u is small compared to the mean-free-path distance λ, so that last term can be neglected. A plot of $\ln(H_u/H_s)$ versus k^2 should therefore produce a straight line with a slope of $\sigma_s^2-\sigma_u^2$ and an intercept of $\ln(N_sA_sR_u^2/N_uA_uR_s^2)$. Using the transferability of the backscattering amplitudes ($A_u\sim A_s$), it is quite straightforward to deduce the coordination number N_u.[49] This technique is known as the ratio method and is outlined in detail in Refs. 35–37, 45, and 50. Choosing a standard with a known structure (crystalline TiB_2) and a chemical environment which is similar to that of the unknown structure (amorphous TiB_2) reduces reliance on the assumption of transferability, and thus allows high accuracy to be achieved in the determination of structural parameters.

Experimentally, the EXAFS and EXELFS spectra appear as low-intensity oscillations (relative to the jump at the absorption or ionization edges) superimposed on the smooth atomic background, which decays with increasing energy above the edge. Typical "raw" EXAFS and EXELFS spectra are shown in Fig. 1 (EXAFS for the Ti K edge in crystalline TiB_2,c-TiB_2) and Fig. 2 (EXELFS for the B K edge and Ti L edges in amorphous TiB_2,a-TiB_2). These data have not been smoothed, or normalized, nor has any background been removed. The figures are only intended to illustrate the excellent signal-to-noise ratio (>300:1) of these data and the quality of μx, where x is the thickness, for the EXAFS and the intensity of the EXELFS spectra achieved from the samples. These excellent signal-counting statistics are essential to produce accurate results and extract correct structural information.

The EXAFS and EXELFS interference functions $\chi(k)$ were extracted from the absorption and energy-loss spectra, respectively, using standard procedures.[36,42,50] The zero of the photoelectron wave vector k was taken to be 4960 eV for the Ti K-edge and 188 eV for the B K-edge spectra. Figures 3 and 4 show the $\chi(k)$ function, weighted by k for the EXAFS data and by k^2 for the EXELFS data, respectively, of the Ti K edges and B K edges in crystalline TiB_2 (standard) and amorphous TiB_2 (unknown). Figure 3(c) is displayed to exhibit the effect of the weighting scheme k^n, which is typically chosen so that the relative importance of the various low-k and high-k regions within the data is appropriately emphasized without severely distoring the amplitude envelope.

The magnitudes of the Fourier transforms or radial distribution functions (RDF's) give the locations and coordination numbers of the surrounding atoms, as shown in Figs. 5 and 6. When the phase shifts $\delta_j(k)$ are not included in the transform, the peaks in the RDF's are shifted. By backtransforming the data over a particular R-space window, the contribution from a single shell can be extracted (Fig. 7). Representative R-space windows of the first and second contribution shells are displayed in Fig. 7(a) for the EXAFS Ti K edge in amorphous TiB_2. The result of this filtering is displayed in Fig. 7(b), where we now show typical filtered single-shell $\chi(k)$ data for the first, $\chi_1(k)$, and second, $\chi_2(k)$, coordination shells sur-

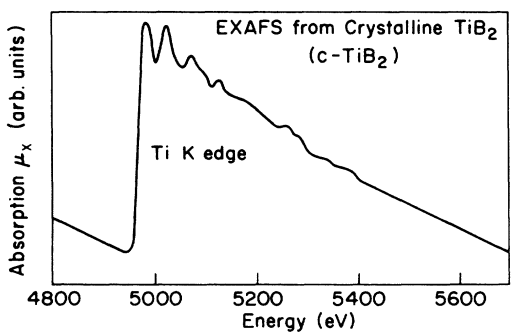

FIG. 1. Typical "raw" x-ray-absorption data, showing EXAFS for the Ti K edge in crystalline TiB_2. Data have not been normalized, smoothed, or edited.

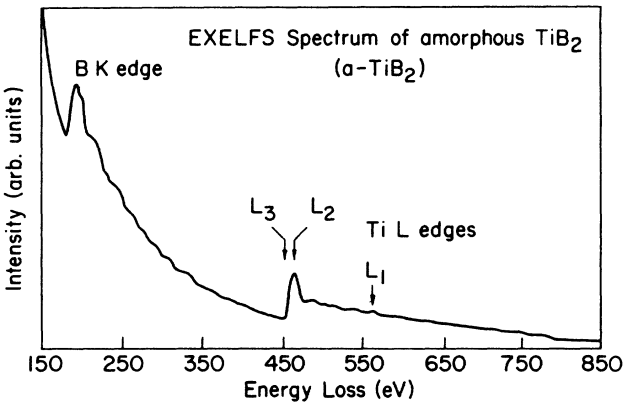

FIG. 2. Typical "raw" electron-energy-loss data, showing EXELFS past the B K edge and the Ti L edges in amorphous TiB_2. Spectra have not been normalized, smoothed, or edited.

rounding a titanium atom in amorphous TiB_2.

Once the single-shell EXAFS and EXELFS data have been isolated, the analysis becomes more specialized. The next step involves breaking down the single-shell $\chi(k)$ data into phase and amplitude parts, then applying the ratio method, as outlined previously in this section. This allows one to compute $\ln(H_u/H_s) = -2k^2(\sigma_s^2 - \sigma_u^2) + \ln(N_s R_u^2/N_u R_s^2)$ and $d\Phi = \Phi_u - \Phi_s = 2k(R_u - R_s)$ for each pair of coordination shells, such as for the titanium first coordination shell in amorphous TiB_2 (the unknown, referred to by the subscript u) and crystalline TiB_2 (the standard, referred to by the subscript s). By

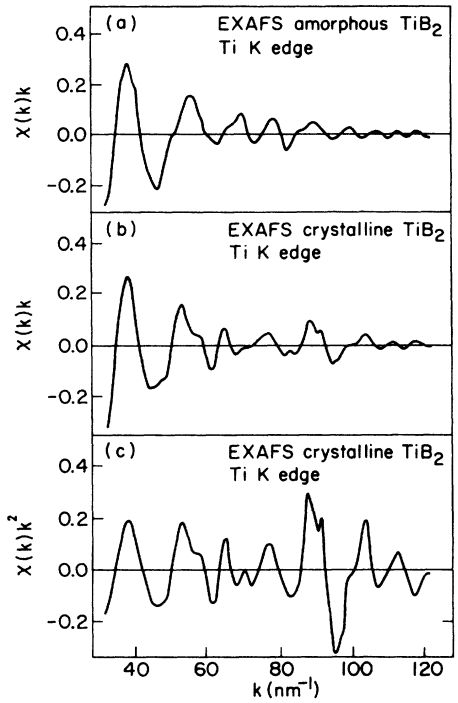

FIG. 3. Isolated EXAFS $\chi(k)k^n$ for the Ti K edge in (a) amorphous TiB_2 ($n=1$), (b) crystalline TiB_2 ($n=1$), and (c) crystalline TiB_2 ($n=2$), all at -195 °C.

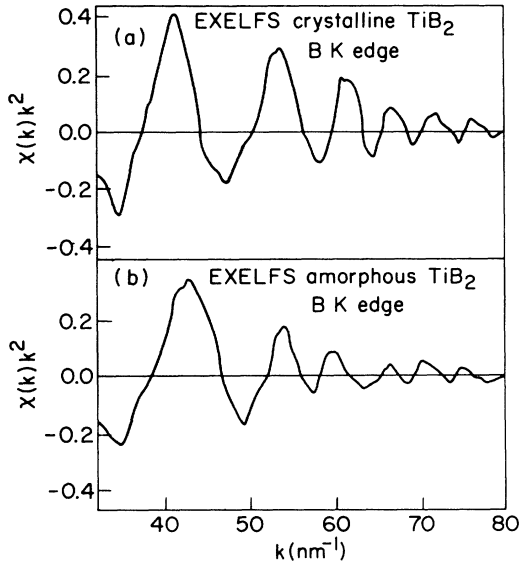

FIG. 4. Isolated EXELFS data $\chi(k)k^2$ at -195° C for the B K edge in (a) crystalline TiB_2 and (b) amorphous TiB_2.

plotting $d\Phi(k)$ versus k, the interatomic distance R_u for the coordination shell under consideration in amorphous TiB_2 is determined from the slope of the straight line; R_s is calculated from crystallographic data for crystalline TiB_2. Debye-Waller-factor deviations $\Delta\sigma^2 = \sigma_s^2 - \sigma_u^2$, and consequently the structural disorder of atoms in coordination shells of amorphous TiB_2 compared to the crystalline standard, and the coordination numbers N_u, are determined from the slope and intercept, respectively, of the plot of $\ln(H_u/H_s)$ versus k^2.

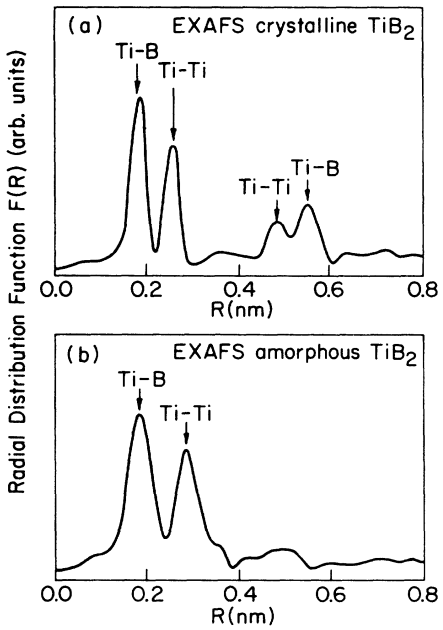

FIG. 5. Fourier transform of EXAFS $\chi(k)$ data from Ti K edge in (a) crystalline TiB_2 (-195 °C) and (b) amorphous TiB_2 (-195 °C).

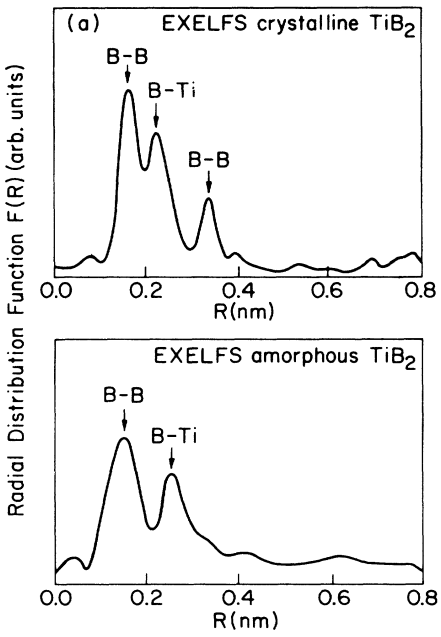

FIG. 6. Fourier transform of EXELFS $\chi(k)$ data from B K edge in (a) crystalline TiB_2 (-195 °C) and (b) amorphous TiB_2 (-195 °C).

Representative phase-difference curves and logarithm (ratio of amplitude envelopes) plots are displayed in Figs. 8 and 9. Figure 8 shows the logarithms of ratio and phase differences [Figs. 8(a) and 8(b), respectively] for the titanium K-edge EXAFS $\chi_1(k)$ data, corresponding to the first coordination shell around a titanium atom in crystalline and amorphous TiB_2. Figure 9 displays the same information from the B K-edge EXELFS $\chi_1(k)$ data, corresponding to the first coordination shell surrounding a boron atom in crystalline and amorphous TiB_2. Deviations of these curves from a straight line at the high-k end of the spectrum are due to noise in the data and to thermal vibrations. As mentioned earlier, the latter were minimized by comparing data for the same measurement temperature (-195 °C). At the low-k end of the spectrum ($k < 30$ nm^{-1}) the nonlinearity observed is attributed mainly to the failure of the EXAFS expression in the XANES—x-ray-absorption near-edge structure—region, ~30–50 eV above the edge. These deviations can be used to estimate the error in ΔR.

Most of the error in the structural determination process is not due to counting statistics or measurement errors, but instead arises from systematics introduced in the analysis process or from inadequacies in the standard EXAFS-EXELFS expression [Eq. (1)], as pointed out by Stern *et al.*[36] and Teo and Lee.[44] Systematic errors in the analysis include uncertainties in the normalization, relative E_0 determination, background distortions introduced by the Fourier filtering, and truncation effects in the Fourier transform. These errors are considered as uncertainties in our results, and their net effect is to make error bars larger at the $k_{\min}$ and $k_{\min}$ ends of the spectra. We minimized these errors appreciably, however, by analyzing the unknown and standard in exactly the same way, and by using the ratio method, which tends to make errors induced by systematics and by many-body effects cancel.[21,45]

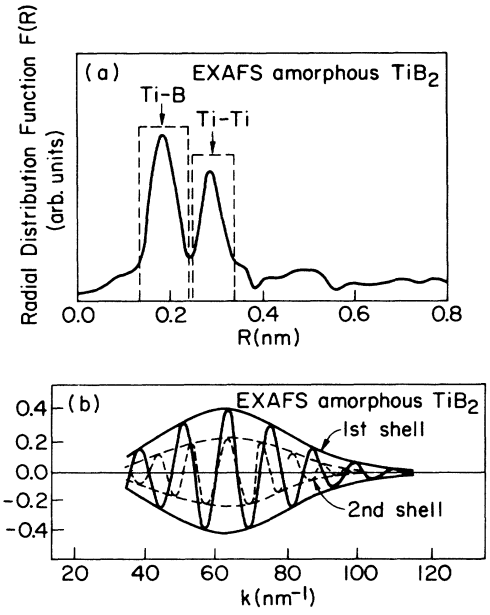

FIG. 7. (a) Typical backtransforming windows for first and second shells in amorphous TiB_2 and (b) single-shell data after backtransforming over a limited range in R space using the R windows shown in (a).

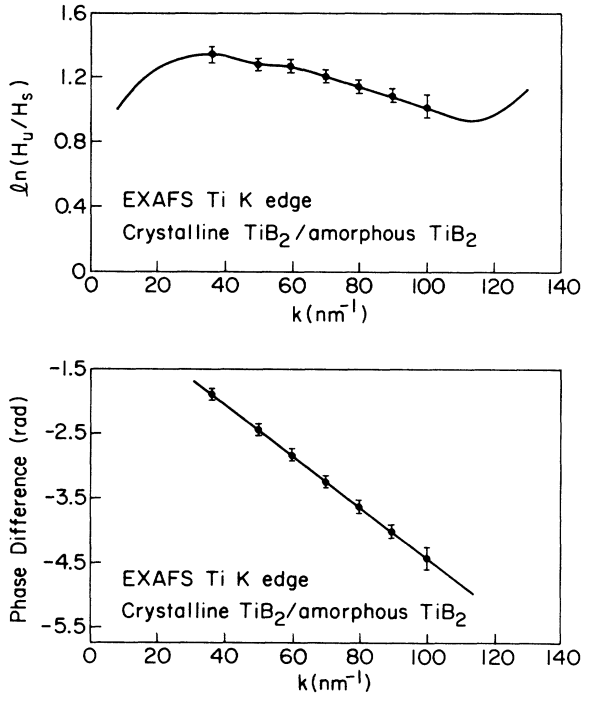

FIG. 8. (a) Logarithm of of amplitudes (H_u/H_s) for the first coordination shell around a Ti atom, from EXAFS Ti K-edge spectra taken at -195 °C, between crystalline TiB_2 and amorphous TiB_2, and (b) the corresponding phase difference. The relative energy zero between both samples, E_0, has been adjusted by 0.6 eV so that the phase intercept at $K=0$ passes through a multiple of $2n\pi$ (Refs. 36 and 45).

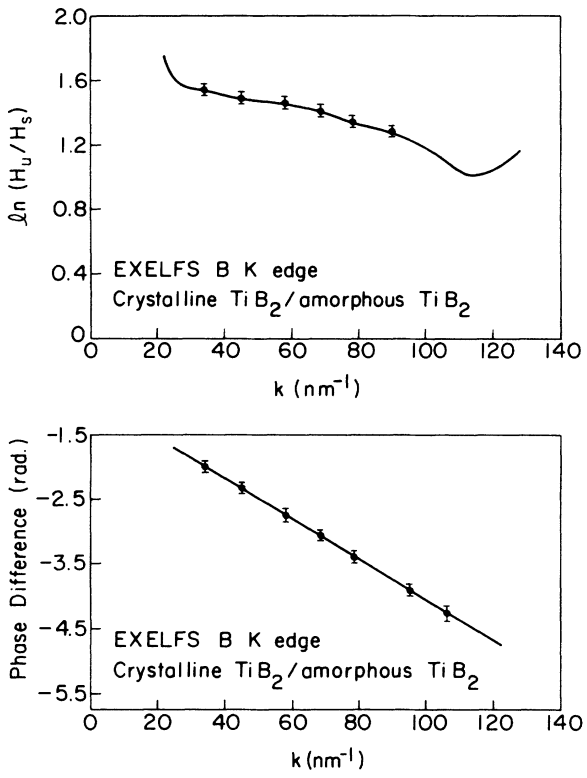

FIG. 9. (a) Logarithm of ratio of amplitudes (H_u/H_s) for the first coordination shell surrounding a B atom, from EXELFS B K-edge spectra taken at $-195\,^{\circ}C$, between crystalline TiB_2 and amorphous TiB_2, and (b) the corresponding phase difference. The relative energy zero was also adjusted (by ~ 0.5 eV) so that the phase intercept at $k=0$ passes through a multiple of $2n\pi$.

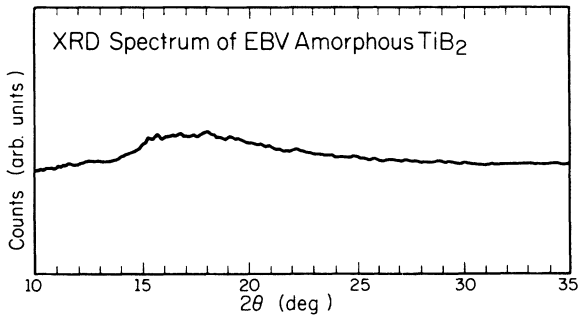

FIG. 10. X-ray-diffraction (XRD) curve for amorphous TiB_2 film produced by EBV.

IV. RESULTS AND DISCUSSION

A. Transmission-electron-microscopy and electron-energy-loss results

Although we expect the deposited film to have the same stoichiometry as the target source, because TiB_2 vaporizes congruently, it is quite straightforward to check this expectation with quantitative EXELFS. The simplicity of such a task emphasizes one of the major advantages of using high-energy electron instead of synchrotron radiation to perform structural studies involving light elements, namely the ability to image the irradiated area, to obtain a selected-area diffraction pattern, and to perform quantitative analysis on the same instrument.[39,51] The value thus obtained for the boron-to-titanium ratio was 2.06 ± 0.10, compared with 2.00.

The x-ray-diffraction (XRD) scans of the film showed that, in $15°-40°$ (2θ) region, only one very broad peak, characteristic of amorphous structures, was detected. This behavior is shown in Fig. 10. Figure 11 displays the selected-area diffraction pattern of the same deposit, obtained during EXELFS data collection. The micrograph shows a few very diffuse rings, which is an additional indication of the amorphicity of the films. The corresponding bright-field image was uniform and featureless, with no grains or microcrystallites detected. However, XRD and selected-area diffraction patterns (SADP's) failed to provide any information on the existence and nature of short-range order (SRO) in the amorphous structure, thus underlying the importance of using EXAFS and EXELFS to provide such structural knowledge.

B. EXAFS-EXELFS results

We were able to obtain structural information for amorphous and crystalline TiB_2 systems with an appreciably higher accuracy than what is typically achieved in similar studies through the use of an absolute calibration procedure presented initially by Boulding, Stern, Von Roedern, and Azoulay.[21,52] The first step in this approach consists of devoting extreme care to eliminating experimental sources of error that include particle-size

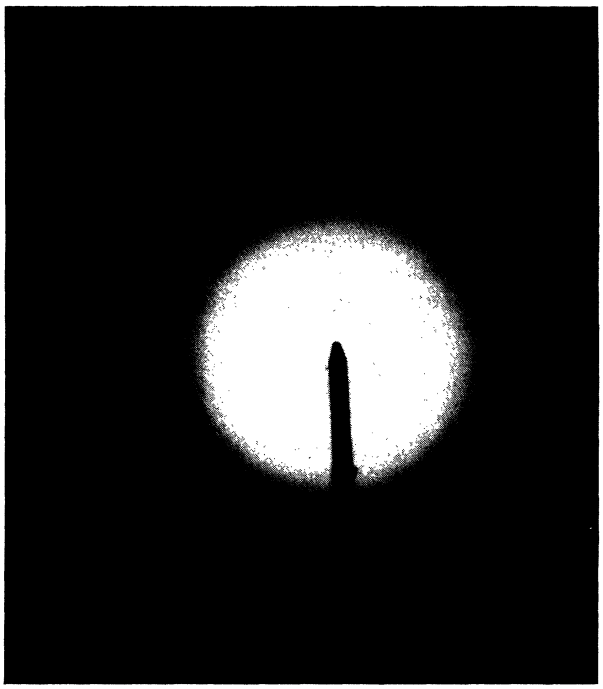

FIG. 11. Selected-area diffraction pattern (SADP) of same film as in Fig. 10 shows few very diffuse rings.

and thickness effects, harmonic contamination in the x-ray beam, etc. A second step involves selecting various sets of experimental parameters and performing measurements to deduce an optimum set—the one that yields the highest signal-to-noise ratio and the best counting statistics. Finally, a consistency check is carried out on a standard material with a known structure to determine the magnitude of errors obtained in the compilation of typical structural parameters such as coordination number N, structural disorder σ^2, etc., and a subsequent absolute calibration of the whole procedure is carried out. We applied this process to three separate standards of crystalline TiB_2, produced by three different experimental techniques. Data for these standards were compiled repeatedly for the Ti K edge using EXAFS and the B K edge using EXELFS, for x-ray- and electron-beam voltages in the range, respectively, 11–13 kV and 200–300 kV, and the whole analysis was subsequently performed for each individual run.

We begin our discussion of the EXAFS-EXELFS results with the experimental observation that truncation ripples are more pronounced in the EXELFS than in the EXAFS radial distribution function, $F(R)$, as seen in Figs. 5 and 6. These artifacts are due to the smaller k range available for Fourier-transforming the EXELFS B K-edge spectra than what is dispensible for the EXAFS Ti K-edge spectra. Nevertheless, by choosing an appropriate Fourier filtering function for analyzing the EXELFS data, we were able to achieve an accuracy comparable to that of the EXAFS data.[45]

The most important observation in Figs. 5 and 6 is that four coordination shells are evident in the radial distribution function about Ti for crystalline TiB_2 [Fig. 5(a)], while only two are seen in the corresponding radial distribution function of amorphous TiB_2 [Fig. 5(b)]. Similarly, at least three coordination shells can be seen in the radial distribution function about B for crystalline TiB_2 [Fig. 6(b)]. The Fourier transforms, therefore, not only agree with the present authors' x-ray- and electron-diffraction findings (Figs. 11 and 12) on the amorphicity of the TiB_2 films; more importantly, they provide accurate information on the local structure and SRO of the films. Such information cannot be acquired by XRD and electron-diffraction (ED) techniques. The EXAFS-EXELFS results show that the amorphous phase is not formed simply of random arrangements of Ti and B atoms that are distributed in a statistical manner in space. Instead, a certain degree of short-range order, which probably plays an important role in defining the properties of amorphous TiB_2, does exist.

The first stage of our study involved employing EXAFS and EXELFS to investigate the conditions for electron-beam vaporization of amorphous TiB_2 as a function of the EBV deposition parameters (electron-beam energy, power rating, etc.). Using structural information provided uniquely by EXAFS and EXELFS, a set of optimized experimental conditions for producing amorphous TiB_2 was then determined. Emphasis was placed on selecting that combination of EBV parameters that would yield a SRO in the amorphous phase with the least nanostructural disorder σ^2 in atomic positions. We believe that the stability of the amorphous structure is strongly dependent on the nature and degree of such disorder and that minimizing σ^2 is crucial in enhancing such stability.

For this purpose, electron-beam (EB) vaporization of amorphous TiB_2 was carried out with the EBV voltage set at, for different deposition runs, values ranging from 6 to 9 kV. The power rating was also varied, for each individual setting of the EB voltage, between 20 and 40 kW in a stepwise manner at 2-kW intervals. The substrates were kept at all times at liquid-nitrogen temperature. The whole EXAFS-EXELFS analysis was subsequently performed for each amorphous film produced, and corresponding radial distribution functions $F(R)$, coordination numbers N, radial distances R, and static disorder factors σ^2 were deduced for the titanium and boron constituents. The data were then compared to those from crystalline TiB_2, used as a standard, and from the other amorphous TiB_2 films. Finally, XRD scans and ED micrographs were collected for each amorphous film produced.

No differences were detected in the amorphous phase for all the EBV-produced TiB_2 films when examined by x-ray and electron diffraction. The XRD scans exhibited the same very broad peak as in Fig. 10, while the ED patterns displayed diffuse, broad halos similar to those in Fig. 11, with both results being characteristic of amorphous systems.

The EXAFS and EXELFS results, on the other hand, showed some interesting changes in the SRO and in the degree of disorder, σ_u^2, of the atomic positions in the amorphous phase with variations in the EBV deposition parameters. In Fig. 12 we display representative curves of $\Delta\sigma^2=\sigma_s^2-\sigma_u^2$ for the first coordination shell surrounding a Ti atom in amorphous TiB_2 films, produced with different depostion parameters, as a function of EB voltage and power rating. The standard used in all these computations is crystalline TiB_2. The observed behavior, which was also exhibited by the second titanium coordi-

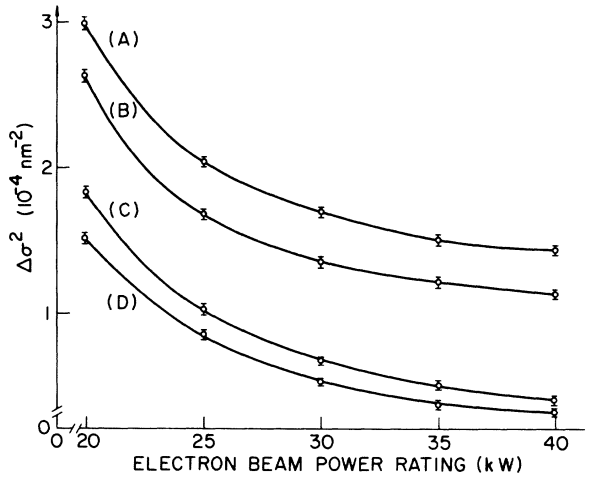

FIG. 12. Change in structural disorder, $\Delta\sigma^2$, of the first coordination shell surrounding a Ti atom in amorphous TiB_2, relative to its counterpart in crystalline TiB_2. $\Delta\sigma^2$ is plotted as a function of the EBV power rating for an electron-beam voltage of (a) 6 kV, (b) 7 kV, (c) 8 kV, and (d) 9 kV.

nation shell and by both boron coordination shells in amorphous TiB_2, is that the degree of disorder in the atomic positions with respect to their crystalline counterparts tends to decrease appreciably with increasing EB voltage and power rating. This observation seems to indicate that an amorphous phase with higher stability is achieved with increased EB voltage and power rating.

By examining the corresponding radial distribution functions $E(R)$, however, we found that for the amorphous films produced with a 9-kV electron beam at a power rating about 30 kW, a third titanium and boron coordination shell starts to appear, as can be seen in Fig. 13. This result seems to indicate that at the higher beam energy and power rating a modified structure with longer range order, the so-called medium-range order,[2] starts to form. It is suggested that this transition from short- to medium-range order—which could be viewed as the threshold for the amorphous-to-crystalline transition—might be attributed to the higher thermal energy available for the vaporized atomic species, namely titanium and boron, at the increased EB voltage and current, which allows migration (atomic rearrangements) to a more ordered phase, and, ultimately, to the crystalline form.

From these observations, two sets of optimum deposition parameters can be proposed for the EBV deposition of a stable amorphous TiB_2 phase, namely 8 kV with 30–40 kW, or 9 kV with 25–30 kW. Lower voltages and currents lead to a highly disordered amorphous structure (see Fig. 13), while higher values lead to medium-range order and possibly crystallization.

The next stage of our analysis involved using the ratio

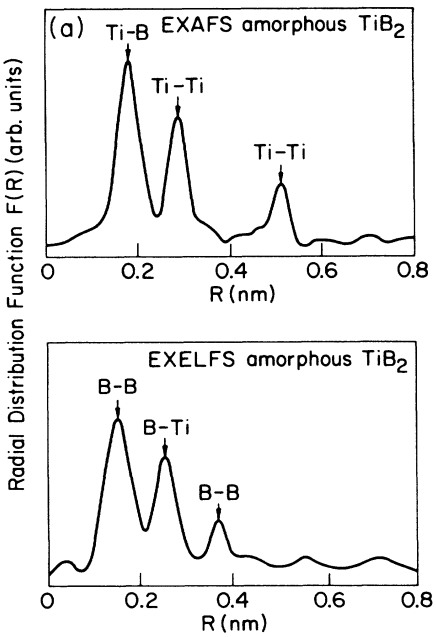

FIG. 13. Typical (a) Ti EXAFS and (b) B EXELFS radial distribution functions $F(R)$ for an amorphous TiB_2 film produced at high EB voltage (9 kV) and increased power rating (>30 kW). A third coordination shell around Ti and B can be detected indicating a transition from short- to medium-range order.

method, with crystalline TiB_2 as a standard, to establish a detailed understanding of the nature of the SRO and to derive accurate information on the coordination number, interatomic distances, and structural disorder for "standard" amorphous TiB_2 films. The films examined are those produced with optimum deposition parameters.

A structural model consistent with the data could be generated by reference to the crystal structure. The crystal structure of TiB_2 is hexagonal with $a=0.3028$ nm and $c=0.3228$ nm; Ti atoms form a simple hexagonal lattice, while B atoms occupy $\frac{1}{6}(2,-2,0,3)$ positions, forming basal planes similar to basal planes in graphite.

The crystalline TiB_2 structure gives the coordination shells listed in Table I. The second coordination shell for Ti includes the six Ti atoms at $a=0.3028$ nm and the two Ti atoms at $c=0.322$ nm, giving an average distance of $(6a+6c)/8=0.3078$ nm. In this context the criterion we are using in defining a coordination shell is based on the common convention that if atoms are separated well enough that their transforms in R space show clearly separated peaks, the atoms are considered to be in different coordination shells; otherwise they are considered to be in the same coordination shell. In practice, this criterion means that atoms more than 0.06 nm apart are considered to be in separated shells.[36]

From the backtransform, coordination shells for the amorphous state are determined. The corresponding coordination numbers and radial distances are also listed in Table I for the Ti and B atoms. There is a general relaxation in the interatomic distances and a reduction in the coordination numbers for amorphous TiB_2. The difference in structural disorder parameters $\sigma_s^2-\sigma_u^2$ [slope of curves in Figs. 8(b) and 9(b)] also shows a disordering trend in going to the amorphous state. In the latter, a fractional coordination number can be interpreted as the average number of atoms occupying a given shell. Since the fundamental structural units in an amorphous solid tend to be arranged so as not to fill space completely, the mismatch in arranging these units might result in a different number of, or a different spacing for, neighboring atoms about some of the reference atoms.

A model can now be proposed for the local structure of amorphous TiB_2. The basic unit in the crystalline state is a prism which has nearly square faces. In the crystal, these units are arranged to fill all space as shown in Fig. 14(a). In the formation of the amorphous state, however,

TABLE I. Interatomic distances and coordination numbers for crystalline and amorphous TiB_2.

Titanium		Boron	
Coord. no.	Distance (nm)	Coord. no.	Distance (nm)
	Crystalline TiB_2		
12 B	0.2337	3 B	0.1748
6 Ti	0.3028	6 Ti	0.2337
2 Ti	0.3228	6 B	0.3028
12 B	0.3851	2 B	0.3228
	Amorphous TiB_2		
10.3 B	0.2355(7)	2.6 B	0.1754(8)
7.3 Ti	0.3275(10)	5.3 Ti	0.2520(9)

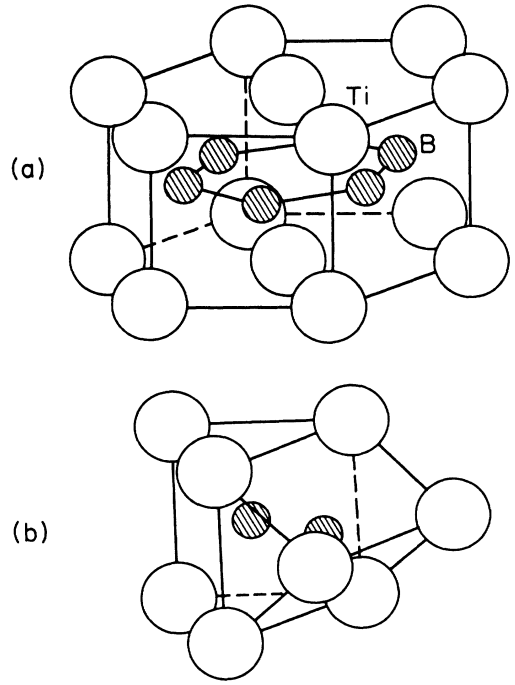

FIG. 14. (a) In crystalline TiB_2 the basic structural unit is prismatic. The prismatic units are arranged with their c axis (vertical direction) parallel; (b) the basic structural unit that seems to exist in amorphous TiB_2. Long-range order is not retained, however, and these units are believed to be randomly arranged in space.

rapid cooling reduces the probability of diffusional jumps required to form the equilibrium phase; individual atoms, upon reaching the substrate, instead build a modified local structural unit, as shown in Fig. 14(b). In this proposed model, relaxation of bonds in the basal plane (a direction) leads to a close correspondence with the bond length in the prismatic plane (c direction)—a difference of only 0.02 nm originally. This value for the required relaxation is approximately what is derived from the EXAFS-EXELFS data. The model, though consistent with the data, is possibly not the only one to fit the data. It needs to be tested by computer simulation, and others may be proposed later in our ongoing investigation. We offer the present model at this preliminary stage of the analysis as one which can rationalize the EXAFS-EXELFS radial distribution functions, $F(R)$.

A problem, however, is associated with the use of the ratio method to derive structural information from systems where a small separation in R space (>0.06 nm) exists between contributing shells of identical atoms. This is the case, e.g., in crystalline TiB_2, where a separation of ~ 0.02 nm is observed between the second and third shells surrounding a Ti atom. The Fourier transform cannot resolve this separation, which leads to a modulation of amplitude and phase that are not included in the ratio method. Consequently, the coordination number and radial distance for the second shell surrounding a Ti atom in amorphous TiB_2 might have larger error bars than those listed in Table I—where we list uncertainties from systematic errors in the analysis, such as relative E_0 determination, truncation effects in the Fourier transform, etc.

For this reason, a deconvolution of the second Ti shell is needed to obtain more accurate phases and amplitudes, and a curve-fitting technique should show details from the subshells in crystalline TiB_2 and detect their existence, if any, in amorphous TiB_2. The EXAFS beats method, proposed by Martens, Rabe, Schwentner, and Werner,[53] seems to be the correct approach. It uses the k values from the extrema in the envelope function and from the inflection points of the phases to calculate the separation of subshells without knowledge of the scattering phases. We will apply this technique at a later stage of our ongoing analysis of amorphous TiB_2.

V. CONCLUSIONS

In summary, we note the following.

(1) Amorphous films of TiB_2 can be prepared by thermal vaporization of the solid compound onto substrates kept at liquid-nitrogen temperature.

(2) The radial distribution function for neighboring atoms about titanium in amorphous and crystalline TiB_2 can be determined by EXAFS and the radial distribution function about boron in amorphous and crystalline TiB_2 by EXELFS. The results showed that the amorphous phase, instead of being characterized by complete randomness, includes some kind of short-range order which extends to the second coordination shell surrounding a Ti or B atom.

(3) There is a general relaxation in the atomic spacing and a reduction in the number of atoms within the coordination shells for amorphous TiB_2 as compared to crystalline TiB_2.

(4) The EXAFS and EXELFS results are consistent with a SRO model of the amorphous form of TiB_2 at this initial stage of our study. The model consists of prismatic structural units on the atomic scale which are similar to those found in the hexagonal crystalline form, but which are rotated and relaxed such that prismatic faces match basal planes. It is possible that this model is not the only one which fits the data, and other models might be proposed at a later stage of our ongoing study.

(5) By examining amorphous TiB_2 films produced by EBV with different deposition parameters (EB voltage, power rating) using EXAFS and EXELFS, sets of optimized experimental conditions for obtaining a stable amorphous phase were determined. These parameters consisted of a beam voltage of 8 kV with a power rating in the range 30–40 kW, or a beam voltage of 9 kV with a power rating in the range 25–30 kW. A highly disordered amorphous structure was produced at lower EB voltages and power ratings, while higher deposition parameters led to medium-range order and possible crystallization.

ACKNOWLEDGMENTS

This work was supported by the University of Illinois at Urbana-Champaign and the U.S. National Science

Foundation under Grant No. MSM-861-17318.

The analyses were carried out in the Center for Microanalysis of Materials of the University of Illinois at Urbana-Champaign Materials Research Laboratory (MRL), which is supported by the U.S. Department of Energy under Contract No. DE-AC02-76ER01198. We thank professional staff members John Woodhouse, Peggy Mochel, Carol Kozlowski, and Nancy Finnegan for instruction in some of the techniques employed. We also extend our appreciation to the staff of the Coordinated Sciences Laboratory glass shop, the Materials Research Laboratory machine shop, and the Loomis Laboratory of Physics electronics shop for their invaluable expertise. Special thanks go to Professor Bruce Bunker and Professor Frederick C. Brown for their extremely helpful suggestions and enlightening discussions.

---

*Present address: Department of Materials Science and Engineering, Case Western Reserve University, Cleveland, OH 44106.

[1]J. Häfner, in *Glassy Metals I: Ionic Structure, Electronic Transport, and Crystallization,* edited by H. Beck and H.-J. Guntherödt (Springer-Verlag, Berlin, 1981), p. 93.

[2]S. R. Elliott, *Physics of Amorphous Materials* (Longmans, London, 1984).

[3]R. Zallen, *The Physics of Amorphous Solids* (Wiley, New York, 1983).

[4]R. Hasegawa, *Glassy Metals: Magnetic, Chemical, and Structural Properties* (Chemical Rubber Co., Boca Raton, FL, 1983).

[5]F. E. Luborsky, in *Amorphous Metallic Alloys,* edited by F. E. Luborsky (Butterworths, London, 1983).

[6]A.E. Kaloyeros, M. P. Hoffman, and W. S. Williams, Thin Solid Films **141**, 237 (1986).

[7]A. E. Kaloyeros and W. S. Williams, Surf. Sci. **171**, L454 (1986).

[8]A. E. Kaloyeros and W. W. Williams, Appl. Phys. A **42**, 139 (1987).

[9]G. S. Girolami, J. A. Jensen, D. M. Pollina, W. S. Williams, A.E. Kaloyeros, and C. M. Allocca, J. Am. Chem. Soc. **109**, 1579 (1987).

[10]A. E. Kaloyeros, W. S. Williams, C. M. Allocca, D. M. Pollina, and G. S. Girolami, Adv. Ceram. Mater. **2**, 100 (1987).

[11]C. M. Allocca, W. S. Williams, and A. E. Kaloyeros, J. Electrochem. Soc. Solid-State Sci. Technol. **134**, 3170 (1987).

[12]K. A. Osipov, E. M. Lazarev, T. L. Borovich, N. A. Korotkov, and N. Yu Yusipov, Izv. Akad. Nauk SSSR, Neorg. Mater. **17**, 631 (1981).

[13]L. M. Williams, Appl. Phys. Lett. **46**, 43 (1985).

[14]T. M. Besmann and K. E. Spear, J. Electrochem. Soc. Solid-State Sci. Technol. **124**, 786 (1977).

[15]T. Takahashi and H. Itoh, J. Cryst. Growth **49**, 445 (1980).

[16]C. Feldman, F. C. Satkiewicz, and G. Jones, J. Less-Common. Met. **79**, 221 (1981).

[17]*Amorphous Materials: Modeling of Structure and Properties,* edited by V. Vitek (The Metallurgical Society of AIME, Warrendale, PA, 1985).

[18]H. D. Pierson and A. W. Mullendore, Thin Solid Films **72**, 511 (1980).

[19]A. J. Caputo, W. J. Lackey, and I. C. Wright, Proc. Electrochem. Soc. **84**, 782 (1984).

[20]H. O. Pierson, E. Randich, and D. M. Mattox, J. Less-Common Met. **67**, 381 (1979).

[21]C. E. Bouldin, E. A. Stern, B. Von Roedern, and J. Azoulay, Phys. Rev. B **30**, 4462 (1984).

[22]M. K. Loudjani, J. Roy, and A. M. Huntz, J. Am. Ceram. Soc. **68**, 559 (1985).

[23]A. W. Searcy, W. S. Williams, and P. O. Schissel, J. Chem. Phys. **32**, 957 (1960).

[24]A. E. Kaloyeros, W. S. Williams, F. C. Brown, A. E. Greene, and J. B. Woodhouse, Phys. Rev. B **37**, 771 (1988).

[25]M. P. Hoffman, Ph.D. thesis, University of Illinois at Urbana-Champaign, 1987.

[26]G. S. Knapp, H. Chen, and T. E. Klippert, Rev. Sci. Instrum. **49**, 1658 (1978); G. S. Knapp, H. H. Pan, P. Georgopoulos, and T. E. Klippert, in *EXAFS and Near-Edge Structure,* edited by A. Bianconi, L. Incoccia, and S. Stipcich (Springer-Verlag, Berlin, 1983), p. 402.

[27]G. S. Knapp and P. Georgopoulos, in *Laboratory EXAFS Facilities—1980,* edited by E. A. Stern (American Institute of Physics, New York, 1980), Chap. 1; E. A. Stern *ibid.* Chap. 4.

[28]P. B. Allen, Solid State Commun. **54**, 929 (1985); N. Alberding and E. D. Cozier, in *EXAFS and Near-Edge Structure III,* edited by K. O. Hodgson, B. Hedman, and J. E. Penner-Hahn (Springer-Verlag, Berlin, 1984), p. 30.

[29]L. Incoccia and S. Modilio, in *EXAFS and Near-Edge Structure,* edited by A. Bianconi, L. Incoccia, and S. Stipcich (Springer-Verlag, Berlin, 1983), p. 91.

[30]M. E. Rose and M. M. Shapiro, Phys. Rev. **74**, 1853 (1948).

[31]K. Q. Lu and E. A. Stern, Nucl. Instrum. Methods **212**, 475 (1983).

[32]R. D. Leapman, P. Rez, and D. F. Mayers, J. Chem. Phys. **72**, 1232 (1980).

[33]R. D. Leapman, L. A. Grunes, P. L. Fejes, and J. Silcox, in *EXAFS Spectroscopy: Techniques and Applications,* edited by B. K. Teo and D. C. Joy (Plenum, New York, 1981), p. 217.

[34]J. Wong, in *Glassy Metals I: Ionic Structure, Electronic Transport, and Crystallization,* edited by H. Beck and H.-J. Guntherödt (Springer-Verlag, Berlin, 1981), p. 45.

[35]E. A. Stern and J. J. Rehr, Phys. Rev. B **27**, 3351 (1983).

[36]D. E. Sayers, E. A. Stern, and F. W. Lytle, Phys. Rev. Lett. **27**, 1024 (1971); E. A. Stern, Phys. Rev. B **10**, 3027 (1974); F. W. Lytle, D. E. Sayers, and E. A. Stern, *ibid.* **11**, 4825 (1975); E. A. Stern, D. E. Sayers, and F. W. Lytle, *ibid.* **11**, 4836 (1975).

[37]E. A. Stern and S. M. Heald, in *Handbook on Synchrotron Radiation,* edited by E. E. Koch (North-Holland, Amsterdam, 1983), p. 955.

[38]B. K. Teo, *EXAFS: Basic Principles and Data Analysis* (Springer-Verlag, Berlin, 1986), p. 21.

[39]S. Csillag, D. E. Johnson, and E. A. Stern, in *EXAFS Spectroscopy: Techniques and Applications,* edited by B. K. Teo and D. C. Joy (Plenum, New York, 1981).

[40]J. Stöhr, in *Emission and Scattering Techniques: Studies of Inorganic Molecules, Solids, and Surfaces,* edited by Peter Day (Reidel, Dordrecht, 1981), p. 213.

[41]R. F. Egerton, *Electron Energy-Loss Spectroscopy in the Electron Microscope* (Plenum, New York, 1986).

[42]R. D. Leapman, in *Microbeam Analysis—1982,* edited by K.

F. J. Heindrich (San Francisco Press, San Francisco, 1982), p. 111.
[43]L. A. Grunes, R. D. Leapman, C. N. Wilker, R. Hoffman, and A. B. Kunz, Phys. Rev. B **25**, 7157 (1982).
[44]B. K. Teo and P. A. Lee, J. Am. Ceram. Soc. **100**, 2815 (1979).
[45]B. Bunker, Ph.D. thesis, University of Washington, Seattle, 1980.
[46]S. M. Heald and E. A. Stern, Synth. Met. **1**, 249 (1980); N. S. Chiu, S. H. Bauer, and M. F. L. Johnson, J. Mol. Struct. **125**, 33 (1984).
[47]P. H. Citrin, Phys. Rev. B **31**, 700 (1985); P. A. Lee and J. B. Pendry, *ibid.* **11**, 2795 (1975).
[48]S. Ainworth and D. P. Woodruff, Solid State Commun. **56**, 461 (1985).
[49]T. Ishii, Prog. Theor. Phys. **72**, 412 (1984).
[50]E. A. Stern, B. Bunker, and S. M. Heald, Phys. Rev. B **21**, 5521 (1980).
[51]D. C. Joy, in *EXAFS Spectroscopy: Techniques and Applications,* edited by B. K. Teo and D. C. Joy (Plenum, New York, 1981), p. 213.
[52]C. E. Bouldin, E. A. Stern, B. Von Roedern, and J. Azoulay, J. Non-Crystl. Solids **66**, 105 (1984).
[53]G. Martens, P. Rabe, N. Schwentner, and A. Werner, Phys. Rev. Lett. **39**, 1411 (1977).

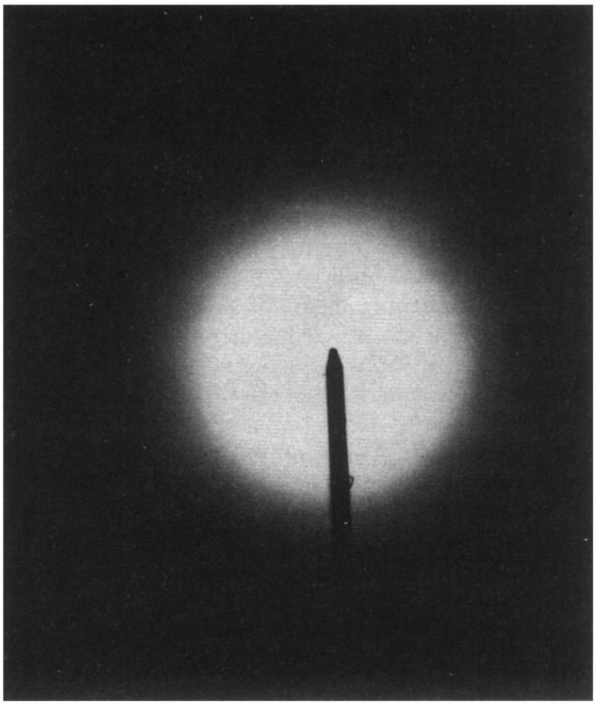

FIG. 11. Selected-area diffraction pattern (SADP) of same film as in Fig. 10 shows few very diffuse rings.